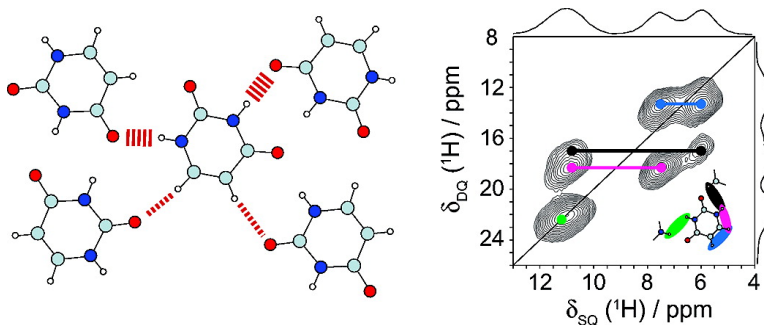


Quantifying Weak Hydrogen Bonding in Uracil and 4-Cyano-4'-ethynylbiphenyl: A Combined Computational and Experimental Investigation of NMR Chemical Shifts in the Solid State

Anne-Christine Uldry, John M. Griffin, Jonathan R. Yates, Marta Prez-Torralba, M. Dolores Santa Mara, Amy L. Webber, Maximus L. L. Beaumont, Ago Samoson, Rosa Mara Claramunt, Chris J. Pickard, and Steven P. Brown

J. Am. Chem. Soc., **2008**, 130 (3), 945-954 • DOI: 10.1021/ja075892i

Downloaded from <http://pubs.acs.org> on February 8, 2009



More About This Article

Additional resources and features associated with this article are available within the HTML version:

- Supporting Information
- Links to the 4 articles that cite this article, as of the time of this article download
- Access to high resolution figures
- Links to articles and content related to this article
- Copyright permission to reproduce figures and/or text from this article

[View the Full Text HTML](#)



Quantifying Weak Hydrogen Bonding in Uracil and 4-Cyano-4'-ethynylbiphenyl: A Combined Computational and Experimental Investigation of NMR Chemical Shifts in the Solid State

Anne-Christine Uldry,[†] John M. Griffin,[‡] Jonathan R. Yates,[§] Marta Pérez-Torrallba,^{||} M. Dolores Santa María,^{||} Amy L. Webber,[‡] Maximus L. L. Beaumont,[‡] Ago Samoson,[⊥] Rosa María Claramunt,^{||} Chris J. Pickard,[†] and Steven P. Brown^{*,‡}

School of Physics and Astronomy, University of St Andrews, North Haugh, St Andrews KY16 9SS, U.K., Department of Physics, University of Warwick, Coventry CV4 7AL, U.K., TCM Group, Cavendish Laboratory, University of Cambridge, 19 J J Thomson Avenue, Cambridge CB3 0HE, U.K., Departamento de Química Orgánica y Bio-Orgánica, UNED, Senda del Rey 9, 28040 Madrid, Spain, and National Institute for Chemical Physics and Biophysics, Akadeemia Tee 23, Tallinn, Estonia

Received August 6, 2007; E-mail: S.P.Brown@warwick.ac.uk

Abstract: Weak hydrogen bonding in uracil and 4-cyano-4'-ethynylbiphenyl, for which single-crystal diffraction structures reveal close CH \cdots O=C and C \equiv CH \cdots N \equiv C distances, is investigated in a study that combines the experimental determination of ^1H , ^{13}C , and ^{15}N chemical shifts by magic-angle spinning (MAS) solid-state NMR with first-principles calculations using plane-wave basis sets. An optimized synthetic route, including the isolation and characterization of intermediates, to 4-cyano-4'-ethynylbiphenyl at natural abundance and with $^{13}\text{C}\equiv^{13}\text{CH}$ and $^{15}\text{N}\equiv\text{C}$ labeling is described. The difference in chemical shifts calculated, on the one hand, for the full crystal structure and, on the other hand, for an isolated molecule depends on both intermolecular hydrogen bonding interactions and aromatic ring current effects. In this study, the two effects are separated computationally by, first, determining the difference in chemical shift between that calculated for a plane (uracil) or an isolated chain (4-cyano-4'-ethynylbiphenyl) and that calculated for an isolated molecule and by, second, calculating intraplane or intrachain nucleus-independent chemical shifts that quantify the ring current effects caused by neighboring molecules. For uracil, isolated molecule to plane changes in the ^1H chemical shift of 2.0 and 2.2 ppm are determined for the CH protons involved in CH \cdots O weak hydrogen bonding; this compares to changes of 5.1 and 5.4 ppm for the NH protons involved in conventional NH \cdots O hydrogen bonding. A comparison of CH bond lengths for geometrically relaxed uracil molecules in the crystal structure and for geometrically relaxed isolated molecules reveals differences of no more than 0.002 Å, which corresponds to changes in the calculated ^1H chemical shifts of at most 0.1 ppm. For the C \equiv CH \cdots N \equiv C weak hydrogen bonds in 4-cyano-4'-ethynylbiphenyl, the calculated molecule to chain changes are of similar magnitude but opposite sign for the donor ^{13}C and acceptor ^{15}N nuclei. In uracil and 4-cyano-4'-ethynylbiphenyl, the CH hydrogen-bonding donors are sp^2 and sp hybridized, respectively; a comparison of the calculated changes in ^1H chemical shift with those for the sp^3 hybridized CH donors in maltose (Yates et al. *J. Am. Chem. Soc.* **2005**, *127*, 10216) reveals no marked dependence on hybridization for weak hydrogen-bonding strength.

1. Introduction

The role of weak C–H \cdots X hydrogen bonding¹ in determining the molecular-level structure and hence a particular property of a material or function of a biological molecule is being increasingly recognized.² For example, recent discussion has

considered the importance of C–H \cdots O hydrogen bonding in protein–ligand binding and drug design,^{3,4} transmembrane helix interactions,^{5–7} and the stability of helical or β -sheet polypeptide structures.^{8,9} Moreover, C–H \cdots O interactions have been shown to play key roles in asymmetric synthesis,¹⁰ the mixing of

[†] University of St Andrews.

[‡] University of Warwick.

[§] Cambridge University.

^{||} UNED Madrid.

[⊥] NICPB, Tallin.

(1) Desiraju, G. R.; Steiner, T. *The Weak Hydrogen Bond in Structural Chemistry and Biology*; Oxford University Press: Oxford, 1999.

(2) Desiraju, G. R. *Chem. Commun.* **2005**, 2995.

(3) Pierce, A. C.; Sandretto, K. L.; Bemis, G. W. *Proteins* **2002**, *49*, 567.

(4) Sarkhel, S.; Desiraju, G. R. *Proteins* **2004**, *54*, 247.

(5) Senes, A.; Ubarretxena-Belandia, I.; Engelman, D. M. *Proc. Natl. Acad. Sci. U.S.A.* **2001**, *98*, 9056.

(6) Loll, B.; Raszewski, G.; Saenger, W.; Biesiadka, J. *J. Mol. Biol.* **2003**, *328*, 737.

(7) Mottamal, M.; Lazaridis, T. *Biochemistry* **2005**, *44*, 1607.

(8) Aravinda, S.; Shamala, N.; Bandyopadhyay, A.; Balaram, P. *J. Am. Chem. Soc.* **2003**, *125*, 15065.

(9) Scheiner, S. *J. Phys. Chem. B* **2006**, *110*, 18670.

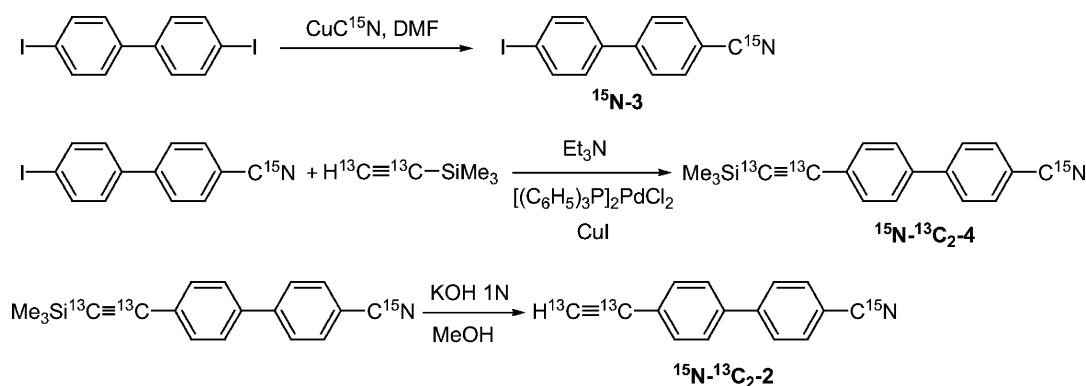
polymers in a blend,¹¹ and the activation of alkane C–H bonds in heterogeneous catalysis.¹² While the existence of some specific weak C–H···X hydrogen bonding interactions has been demonstrated by spectroscopic techniques, e.g., pioneering gas-phase infrared measurements^{13,14} as well as recent Fourier transform infrared (FTIR) experiments on lipid bilayers¹⁵ and a gas-phase photoelectron spectroscopic investigation of aliphatic carboxylate molecules,¹⁶ most evidence for the existence of weak C–H···X hydrogen bonds has been provided by analysis of high-resolution crystal structures obtained by X-ray or neutron diffraction.¹⁷ In particular, the widespread occurrence of short C–H···X distances in molecular crystals^{6,18–21} is taken to represent strong support for such close C–H···X contacts constituting bonding interactions. The question, however, remains as to whether these close contacts between potential donors and acceptors are indeed bonding interactions that contribute to stabilizing the structure or are merely accidental, as a result of other packing constraints.²² For example, an experimental study of the thermodynamic stability of the membrane protein bacteriorhodopsin showed that mutations which remove a putative CH···O hydrogen bond (CHO angle = 117° and C–O distance = 3.4 Å) did not cause significant destabilization.²³

The Nuclear Magnetic Resonance (NMR) chemical shift is a sensitive indicator of the local electronic environment, thus suggesting its suitability as a probe of weak hydrogen bonding. Indeed, in solution-state NMR, an investigation of serine protease catalysis revealed that the C_ε¹–H_ε¹ proton chemical shift for the catalytic histidine is shifted by ~0.6 to 0.8 ppm downfield because of C–H···O hydrogen bonding,²⁴ while Solà et al.¹⁰ have observed a downfield shift of 2.1 ppm of a CH ¹H resonance between the syn and anti conformers of an organometallic complex, with intramolecular C–H···O hydrogen bonding only being possible in the former case. Moreover, Cordier et al. have measured ⁴³J_{CαC} couplings of 0.2 to 0.3 Hz across C^α–H^α···O=C hydrogen bonds in β-sheet regions of a small protein.²⁵ In the solid state, it has been shown that the ¹H NMR chemical shift is a powerful probe of the intermolecular interactions, notably hydrogen bonding and π–π interactions, that control the self-assembly of organic molecules in the solid state.²⁶ Specifically, proton–proton proximities are identified in two-dimensional ¹H double-quantum (DQ) correlation spectra recorded under fast magic-angle spinning (MAS)^{27,28} or using

a combined rotation and multiple-pulse sequence (CRAMPS) approach,^{29–31} with applications including the study of structure and dynamics in hydrogen-bonded polymers³² and the biological molecule bilirubin,³³ π–π stacked polycyclic aromatic systems,^{34–36} polyoxoniobate materials,³⁷ proton-conducting materials,³⁸ and surface organometallic species.^{39,40} Moreover, it is being increasingly recognized that valuable insight is provided by combining experiment with chemical shift calculations.^{41–64} In the context of weak hydrogen bonding, Yates et al. showed, for the case of maltose anomers, that the strength of weak C–H···O hydrogen bonding can be quantified by determining the

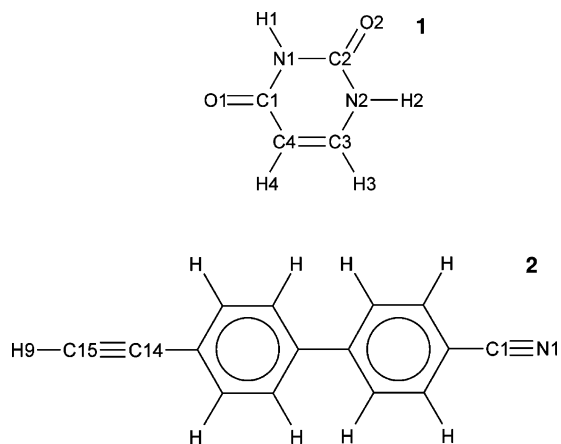
- (10) Solà, J.; Riera, A.; Vardaguer, X.; Maestro, M. A. *J. Am. Chem. Soc.* **2005**, *127*, 13629.
- (11) Green, M. M.; White, J. L.; Mirau, P.; Scheinfeld, M. H. *Macromolecules* **2006**, *39*, 5971.
- (12) Sremaniak, L. S.; Whitten, J. L.; Truitt, M. J.; White, J. L. *J. Phys. Chem. B* **2006**, *110*, 20762.
- (13) Allerhand, A.; von Rague Schleyer, P. J. *Am. Chem. Soc.* **1963**, *85*, 1715.
- (14) Sutor, D. J. *J. Chem. Soc.* **1963**, 1105.
- (15) Arbely, E.; Arkin, I. T. *J. Am. Chem. Soc.* **2004**, *126*, 5362.
- (16) Wang, X.-B.; Woo, H.-K.; Kiran, B.; Want, L.-S. *Angew. Chem., Int. Ed.* **2005**, *44*, 4968.
- (17) Steiner, T. *Cryst. Rev.* **2003**, *9*, 177.
- (18) Taylor, R.; Kennard, O. *J. Am. Chem. Soc.* **1982**, *104*, 5063.
- (19) Steiner, T.; Saenger, W. *J. Am. Chem. Soc.* **1992**, *114*, 10146.
- (20) Derewenda, Z. S.; Lee, L.; Derewenda, U. *J. Mol. Biol.* **1995**, *252*, 248.
- (21) Esposito, L.; Vitagliano, L.; Sica, F.; Sorrentino, G.; Zagari, A.; Mazzarella, L. *J. Mol. Biol.* **2000**, *297*, 713.
- (22) Dunitz, J. D.; Gavezzotti, A. *Angew. Chem., Int. Ed.* **2005**, *44*, 1766.
- (23) Yohannan, S.; Faham, S.; Yang, D.; Grosfeld, D.; Chamberlain, A. K.; Bowie, J. U. *J. Am. Chem. Soc.* **2004**, *126*, 2284.
- (24) Ash, E. L.; Sudmeier, J. L.; Day, R. M.; Vincen, M.; Torchilin, E. V.; Haddad, K. C.; Bradshaw, E. M.; Sanford, D. G.; Bachovchin, W. W. *Proc. Natl. Acad. Sci. U.S.A.* **2000**, *97*, 10371.
- (25) Cordier, F.; Barfield, M.; Grzesiek, S. *J. Am. Chem. Soc.* **2003**, *125*, 15750.
- (26) Brown, S. P.; Spiess, H. W. *Chem. Rev.* **2001**, *101*, 4125.
- (27) Schnell, I. *Prog. Nucl. Magn. Reson. Spectrosc.* **2004**, *45*, 145.
- (28) Brown, S. P. *Prog. Nucl. Magn. Reson. Spectrosc.* **2007**, *50*, 199.
- (29) Hafner, S.; Spiess, H. W. *Solid State Nucl. Magn. Reson.* **1997**, *8*, 17.
- (30) Madhu, P. K.; Vinogradov, E.; Vega, S. *Chem. Phys. Lett.* **2004**, *394*, 423.
- (31) Brown, S. P.; Lesage, A.; Elena, B.; Emsley, L. *J. Am. Chem. Soc.* **2004**, *126*, 13230.
- (32) Schnell, I.; Brown, S. P.; Low, H. Y.; Ishida, H.; Spiess, H. W. *J. Am. Chem. Soc.* **1998**, *120*, 11784.
- (33) Brown, S. P.; Zhu, X. X.; Saalwachter, K.; Spiess, H. W. *J. Am. Chem. Soc.* **2001**, *123*, 4275.
- (34) Brown, S. P.; Schnell, I.; Brand, J. D.; Mullen, K.; Spiess, H. W. *J. Am. Chem. Soc.* **1999**, *121*, 6712.
- (35) Brown, S. P.; Schnell, I.; Brand, J. D.; Mullen, K.; Spiess, H. W. *J. Mol. Struct.* **2000**, *521*, 179.
- (36) Brown, S. P.; Schnell, I.; Brand, J. D.; Mullen, K.; Spiess, H. W. *Phys. Chem. Chem. Phys.* **2000**, *2*, 1735.
- (37) Alam, T. M.; Nyman, M.; Cherry, B. R.; Segall, J. M.; Lybarger, L. E. *J. Am. Chem. Soc.* **2004**, *126*, 5610.
- (38) Traer, J. W.; Montoneri, E.; Samoson, A.; Past, J.; Tuhern, T.; Goward, G. R. *Chem. Mater.* **2006**, *18*, 4747.
- (39) Rataboul, F.; Baudouin, A.; Thieuleux, C.; Veyre, L.; Coperet, C.; Thivolle-Cazat, J.; Basset, J. M.; Lesage, A.; Emsley, L. *J. Am. Chem. Soc.* **2004**, *126*, 12541.
- (40) Avenier, P.; Lesage, A.; Taoufik, M.; Baudouin, A.; De Mallmann, A.; Fiddy, S.; Vautier, M.; Veyre, L.; Basset, J. M.; Emsley, L.; Quadrelli, E. A. *J. Am. Chem. Soc.* **2007**, *129*, 176.
- (41) Ochsenfeld, C.; Brown, S. P.; Schnell, I.; Gauss, J.; Spiess, H. W. *J. Am. Chem. Soc.* **2001**, *123*, 2597.
- (42) Brown, S. P.; Schaller, T.; Seelbach, U. P.; Koziol, F.; Ochsenfeld, C.; Klärner, F.-G.; Spiess, H. W. *Angew. Chem., Int. Ed.* **2001**, *40*, 717.
- (43) Ochsenfeld, C.; Koziol, F.; Brown, S. P.; Schaller, T.; Seelbach, U. P.; Klärner, F.-G. *Solid State Nucl. Magn. Reson.* **2002**, *22*, 128.
- (44) Goward, G. R.; Schuster, M. F. H.; Sebastiani, D.; Schnell, I.; Spiess, H. W. *J. Phys. Chem. B* **2002**, *106*, 9322.
- (45) Goward, G. R.; Sebastiani, D.; Schnell, I.; Spiess, H. W.; Kim, H. D.; H., I. *J. Am. Chem. Soc.* **2003**, *125*, 5792.
- (46) Harris, R. K.; Chi, P. Y.; Hammond, R. B.; Ma, C. Y.; Roberts, K. J. *Chem. Commun.* **2003**, 2834.
- (47) Sebastiani, D.; Rothlisberger, U. *J. Phys. Chem. B* **2004**, *108*, 2807.
- (48) Hoffman, A.; Sebastiani, D.; Sugiono, E.; Yun, S.; Kim, K. S.; Spiess, H. W.; Schnell, I. *Chem. Phys. Lett.* **2004**, *388*, 164.
- (49) Harris, R. K. *Solid State Sci.* **2004**, *6*, 1025.
- (50) Gervais, C.; Profeta, M.; Lafond, V.; Bonhomme, C.; Azaïs, T.; Mutin, H.; Pickard, C. J.; Mauri, F.; Babonneau, F. *Magn. Reson. Chem.* **2004**, *42*, 445.
- (51) Yates, J. R.; Pham, T. N.; Pickard, C. J.; Mauri, F.; Amado, A.; Gil, A. M.; Brown, S. P. *J. Am. Chem. Soc.* **2005**, *127*, 10216.
- (52) Schulz-Dobrick, M.; Metzroth, T.; Spiess, H. W.; Gauss, J.; Schnell, I. *ChemPhysChem* **2005**, *6*, 315.
- (53) Yates, J. R.; Dobbins, S. E.; Pickard, C. J.; Mauri, F.; Ghi, P. Y.; Harris, R. K. *Phys. Chem. Chem. Phys.* **2005**, *7*, 1402.
- (54) Gobetto, R.; Nervi, C.; Valfre, E.; Chierotti, M. R.; Braga, D.; Maini, L.; Greponi, F.; Harris, R. K.; Ghi, P. Y. *Chem. Mater.* **2005**, *17*, 1457.
- (55) Harris, R. K.; Ghi, R. B.; Hammond, R. B.; Ma, C. Y.; Roberts, K. J.; Yates, J. R.; Pickard, C. J. *Magn. Reson. Chem.* **2006**, *44*, 325.
- (56) Schmidt, J.; Hoffmann, A.; Spiess, H. W.; Sebastiani, D. *J. Phys. Chem. B* **2006**, *110*, 23204.
- (57) Heine, T.; Corminboeuf, C.; Grossmann, G.; Haeberlen, U. *Angew. Chem., Int. Ed.* **2006**, *45*, 7292.
- (58) Mifsud, N.; Elena, B.; Pickard, C. J.; Lesage, A.; Emsley, L. *Phys. Chem. Chem. Phys.* **2006**, *8*, 3418.
- (59) Schaller, T.; Büchele, U. P.; Klärner, F.-G.; Bläser, D.; Boese, R.; Brown, S. P.; Spiess, H. W.; Koziol, F.; Kussmann, J.; Ochsenfeld, C. *J. Am. Chem. Soc.* **2007**, *129*, 1293.
- (60) Wiench, J. W.; Avadhut, Y. S.; Maity, N.; Bhaduri, S.; Lahiri, G. K.; Pruski, M.; Ganapathy, S. *J. Phys. Chem. B* **2007**, *111*, 3877.
- (61) Elena, B.; Pintacuda, G.; Mifsud, N.; Emsley, L. *J. Am. Chem. Soc.* **2006**, *128*, 9555.
- (62) Gervais, C.; Coelho, C.; Azaïs, T.; Maquet, J.; Laurent, G.; Pourpoint, F.; Bonhomme, C.; Florian, P.; Alonso, B.; Guerrero, G.; Mutin, P. H.; Mauri, F. *J. Magn. Reson.* **2007**, *187*, 131.
- (63) Brunklaus, G.; Koch, A.; Sebastiani, D.; Spiess, H. W. *Phys. Chem. Chem. Phys.* **2007**, *9*, 4545.
- (64) Zienau, J.; Kussmann, J.; Koziol, F.; Ochsenfeld, C. *Phys. Chem. Chem. Phys.* **2007**, *9*, 4552.

Scheme 1



difference in ^1H chemical shift between calculations for the periodic crystal structure and an isolated molecule.⁵¹ A key result from this study was the observation of a clear correlation between large chemical shift differences (up to 2 ppm) and both short intermolecular $\text{H}\cdots\text{O}$ distances and bonding angles larger than 130° . This observation is consistent with the finding by Yohannan et al.²³ that a $\text{CH}\cdots\text{O}$ contact with a short $\text{H}\cdots\text{O}$ distance, but an unfavorable CHO angle (117°), did not make a significant contribution to the stability of bacteriorhodopsin.

In 1963, Allerhand and Schleyer postulated that the strength of a weak hydrogen bonding interaction depends on the hybridization of the $\text{C}-\text{H}$ donor group, i.e., $\text{C}(sp)-\text{H} > \text{C}(sp^2)-\text{H} > \text{C}(sp^3)-\text{H}$.^{1,13,17} In this paper, the effect of hybridization is investigated by applying a combined experimental and computational approach to two compounds, uracil **1** and 4-cyano-4'-ethynylbiphenyl **2**. In uracil, the weak



hydrogen bond donors are sp^2 $\text{C}-\text{H}$ groups with $\text{C}=\text{O}$ carbonyl oxygens as acceptors; indeed, uracil was included in the pioneering systematic crystallographic investigation of $\text{C}-\text{H}\cdots\text{O}$ interactions in purine and pyrimidine systems by Sutor in 1963.¹⁴ In 4-cyano-4'-ethynylbiphenyl, for which IR spectroscopy shows evidence for weak hydrogen bonding,⁶⁵ the donors are sp hybridized alkyne $\text{C}-\text{H}$ groups and the acceptors are $\text{C}\equiv\text{N}$ groups. As noted by Langley et al.,⁶⁵ the $\text{C}\equiv\text{CH}\cdots\text{N}\equiv\text{C}$ synthon is identical to that observed in cyanoacetylene in 1958.⁶⁶ In this way, this investigation complements our initial work on the maltose anomers,⁵¹ where the $\text{C}-\text{H}\cdots\text{O}$ hydrogen

bonding donors are sp^3 hybridized with OH hydroxyl moieties as acceptor groups. A further important aspect of this work is the presentation of computational methods for separately determining the contribution to the NMR chemical shift of intermolecular hydrogen bonding and intermolecular ring current effects, as is required for uracil and 4-cyano-4'-ethynylbiphenyl, where, as is commonly the case, the molecules contain aromatic moieties as well as hydrogen-bonding groups.

2. Experimental and Computational Details

2.1. Materials and Synthesis. Natural abundance and ^{15}N -labeled ($>99\%$) uracil (**1**) was obtained from Sigma-Aldrich, U.K., and Cambridge Isotope Laboratories, Andover, MA, USA, respectively, and used without further purification. While the preparation and characterization of **2** at natural abundance has been reported in ref 65, the synthetic procedure was not described in detail, with specifically no details being given concerning either the isolation or characterization of the intermediate compound **4** (see Scheme 1); the authors simply stated that it was obtained according to the Hagihara et al. conditions.⁶⁷ We describe here an optimized synthetic route to unlabeled and labeled **2** according to the three-step method depicted in Scheme 1. Specifically, 4-(^{15}N)cyano-4'-iodobiphenyl (^{15}N -**3**) was obtained by reaction of commercially obtainable 4,4'-diiodobiphenyl with (^{15}N)-cuprous cyanide in dimethylformamide⁶⁸ and subsequently treated with trimethylsilyl-($^{13}\text{C}_2$)acetylene in the presence of catalytic amounts of bis[triphenylphosphine]palladium(II) dichloride and copper(I) iodide in triethylamine to afford 4-(^{15}N)cyano-4'-[(trimethylsilyl)($^{13}\text{C}_2$)ethynyl]biphenyl ($^{15}\text{N}-^{13}\text{C}_2$ -**4**). Final hydrolysis with dilute aqueous potassium hydroxide in methanol gives rise to ($^{15}\text{N}-^{13}\text{C}_2$ -**2**). Full details are given in the Supporting Information, where IUPAC nomenclature for each compound has also been included.

2.2. Solid-State NMR. ^{13}C and ^{15}N cross-polarization (CP) MAS experiments were performed on a Varian Infinity Plus spectrometer operating at ^1H , ^{13}C , and ^{15}N Larmor frequencies of 300, 75.5, and 30.4 MHz, respectively, using a Bruker 4 mm double resonance probe at a MAS frequency of 8.5 kHz. Ramped cross polarization^{69,70} from ^1H was used to create transverse ^{13}C and ^{15}N magnetization, with contact times of 1.0 and 3.0 ms, respectively. The ^1H 90° pulse length was of duration 2.5 μs . TPPM decoupling⁷¹ at a ^1H nutation frequency of 100 kHz was applied during acquisition, using pulse lengths of 4.67 μs and a relative phase shift of 11.2° (as determined by a direct spectral

(65) Langley, P. J.; Hulliger, J.; Thaimattam, R.; Desiraju, G. R. *New J. Chem.* **1998**, *22*, 1307.

(66) Schallcross, F. V.; Carpenter, G. B. *Acta Crystallogr.* **1958**, *11*, 490.

(67) Takahashi, S.; Kuroyama, Y.; Sonogashira, K.; Hagihara, N. *Synthesis* **1980**, 627.

(68) McNamara, J. M.; Gleason, W. B. *J. Org. Chem.* **1976**, *41*, 1071.

(69) Hediger, S.; Meier, B. H.; Kurur, N. D.; Bodenhausen, G.; Ernst, R. R. *Chem. Phys. Lett.* **1994**, *223*, 283.

(70) Metz, G.; Wu, X. L.; Smith, S. O. *J. Magn. Reson., Ser. A* **1994**, *110*, 219.

(71) Bennett, A. E.; Rienstra, C. M.; Auger, M.; Lakshmi, K. V. *J. Chem. Phys.* **1995**, *103*, 6951.

optimization approach).^{72–74} Recycle delays of 16 s (**1**), 16 s (**2**, ¹³C), and 128 s (**2**, ¹⁵N) were used.

The rotor-synchronized two-dimensional ¹H double-quantum (DQ) MAS experiments^{26–28} were performed on a Bruker Avance II+ spectrometer, operating at a ¹H Larmor frequency of 600 MHz. The experiments were performed at a MAS frequency of 40 kHz, using a specially developed 1.8 mm double-resonance probe.⁷⁵ (The probe is fitted with a cooling port, such that the additional frictional temperature increase, as has been previously calibrated, is only +15 °C.) The pulse sequence and coherence-transfer pathway diagram for the employed z-filtered DQ MAS experiment is shown in Figure 7 of ref 26. One cycle of the BABA⁷⁶ dipolar recoupling sequence was used to create DQ coherence. The ¹H 90° pulse length was of duration 2.5 μs. A 16-step phase cycle was used to select $\Delta p = \pm 2$ on the DQ excitation pulses (4 steps) and $\Delta p = -1$ (4 steps) on the z-filter 90° pulse, where p is the coherence order. Sign discrimination in the indirect dimension was achieved using the States⁷⁷ protocol. 16 transients were coadded for each of 88 (**1**) or 144 (**2**) t_1 slices. Recycle delays of 10 and 40 s were used for **1** and **2**, respectively.

¹H and ¹³C chemical shifts are indirectly referenced relative to neat tetramethyl silane (Si(CH₃)₄), using the CH₃ resonance of powdered L-alanine (1.1 ppm (¹H) and 20.5 ppm (¹³C)) as an external reference, equivalent to adamantane ¹³C resonances at 29.5 and 38.5 ppm.^{78,79} ¹⁵N chemical shifts are indirectly referenced relative to neat liquid CH₃-NO₂, by using the ¹⁵N resonance of powdered glycine at -347.4 ppm as an external reference. To convert to the chemical shift scale frequently used in protein NMR, where the reference is liquid ammonia at -50 °C, it is necessary to add 379.5 to the given values.

2.3. Computational Details. The first-principles calculations were performed with the academic release version 4.1 of the CASTEP⁸⁰ software package, which implements density functional theory using a plane-wave basis set. The calculations of the shielding tensor utilize the gauge-including projector augmented-wave method⁸¹ (GIPAW) with “ultrasoft” pseudopotentials,⁸² as developed by Yates et al.⁸³

The crystal structures of uracil and 4-cyano-4'-ethynylbiphenyl were obtained from the Cambridge Crystal Database⁸⁴ (database reference code URACIL and JOQSEN, respectively). Geometry optimizations were performed using the PBE⁸⁵ exchange-correlation functional and ultrasoft pseudopotentials with a basis set cutoff at 1200 eV and a 2 × 2 × 4 Monkhorst–Pack grid for uracil, and 522 eV with a 2 × 1 × 1 Monkhorst–Pack grid for 4-cyano-4'-ethynylbiphenyl. The high cutoff chosen for uracil is required by the presence of the oxygen, for which even the ultrasoft pseudopotential is relatively hard. Note however that a lower level of convergence would not affect significantly the conclusions drawn in this work. Since non-negligible residual forces remained on the other atoms after first relaxing only the protons (up to 1.2 eV/Å for uracil and 4.7 eV/Å for 4-cyano-4'-ethynylbiphenyl), all the atoms in the unit cell were subsequently relaxed.

For uracil, shielding tensors were calculated (see below) for isolated planes and isolated molecules as well as for the fully geometrically

relaxed crystal structure. Keeping the atoms in their crystal positions, i.e., without further geometric relaxation, the distance between single planes was progressively increased until the shieldings converge to within 0.04 ppm, effectively isolating one plane from another. This occurred at a separation of 31 Å, which corresponds to ~10 times the size of the original unit cell along the out-of-plane direction. The single molecule was put into a 8000 Å³ cell, such that intermolecular interactions with its neighbors are negligible. For 4-cyano-4'-ethynylbiphenyl, shieldings were calculated for isolated chains and molecules. Four distinguishable chains were first taken out of the relaxed crystal structure. The molecules in the chains were then spaced out so as to effectively isolate each one from external influence. Specifically, the chains were calculated in a 25 × b × 25 Å³ cell, where b is the original crystal lattice parameter of the side along which the chains are aligned. The separated molecules were put in a 25 × 27 × 25 Å³ cell.

For both uracil and 4-cyano-4'-ethynylbiphenyl, the effect of intermolecular interactions on the bond lengths was investigated by relaxing the isolated molecules (starting with the isolated molecule arrangements described above). In uracil, all atoms were relaxed. For 4-cyano-4'-ethynylbiphenyl, the values cited in the main text are those obtained by relaxing the protons only. (A full relaxation of all the atoms was however also performed, the results of which are given in the Supporting Information.) The geometry-optimizations were performed with the cutoff energy at 1100 eV (uracil) or 600 eV (4-cyano-4'-ethynylbiphenyl) and a single k-point at the fractional coordinate (0.25, 0.25, 0.25).

For the geometrically relaxed arrangements described above, shielding tensors were calculated for all atoms. For the uracil crystal the parameters used were a Brillouin zone sampling defined by a 3 × 3 × 8 Monkhorst–Pack grid and a plane-wave cutoff at 1100 eV. This corresponded to the values of the isotropic shielding σ_{iso} being converged to ±0.01 ppm for the protons and ±0.05 ppm for the other atoms. Shieldings in 4-cyano-4'-ethynylbiphenyl were obtained with a 3 × 2 × 2 Monkhorst–Pack grid and a cutoff energy of 560 eV. For the isolated planes/chains and molecules, a single k-point at the fractional coordinate (0.25, 0.25, 0.25) was found to be sufficient with a plane-wave energy cutoff of 1100 eV (uracil) or 600 eV (4-cyano-4'-ethynylbiphenyl).

Nucleus-Independent Chemical Shifts⁸⁶ (NICSSs) were determined in order to estimate the contribution from aromatic ring currents on neighboring molecules. The shieldings in CASTEP are obtained from the calculation of the first-order-induced current that is generated by the application of the magnetic field.⁸¹ The induced current is computed in reciprocal space, and the shielding can thus be obtained at any point of the real space. It is therefore straightforward to calculate the NICSSs, defined as $-\sigma_{\text{iso}}$, anywhere in the unit cell. In this work, the NICSSs were calculated within the isolated uracil plane, and within the isolated 4-cyano-4'-ethynylbiphenyl chains, using the same calculation parameters as those used for the shielding values at the nuclei. Note that, for the compounds under consideration in this work, only the nearest rings, within a plane or a chain, give a significant contribution (which from ring currents are expected to drop off with distance as $1/r^3$). This is evident from the calculations performed on the isolated molecules. In the case of **2**, the single molecules are fully isolated from one another when the ethynyl proton and the closest neighbor's ring is 17 Å apart. In the chain configuration, the second nearest neighbor's ring is 22 Å away, excluding therefore any contribution from that ring. As for the uracil, it will be seen that even the nearest neighbor rings do not contribute significantly.

The chemical shift $\delta_{\text{iso}} = \sigma_{\text{ref}} - \sigma_{\text{iso}}$ is given with respect to a reference (e.g., TMS for ¹H and ¹³C). The references for carbon and

- (72) De Paepe, G.; Hodgkinson, P.; Emsley, L. *Chem. Phys. Lett.* **2003**, *376*, 259.
 (73) De Paepe, G.; Giraud, N.; Lesage, A.; Hodgkinson, P.; Bockmann, A.; Emsley, L. *J. Am. Chem. Soc.* **2003**, *125*, 13938.
 (74) Pileio, G.; Guo, Y.; Pham, T. N.; Griffin, J. M.; Levitt, M. H.; Brown, S. P. *J. Am. Chem. Soc.* **2007**, *129*, 10972.
 (75) Samoson, A.; Turhem, T.; Past, J. *J. Magn. Reson.* **2001**, *149*, 264.
 (76) Sommer, W.; Gottwald, J.; Demco, D. E.; Spiess, H. W. *J. Magn. Reson., Ser. A* **1995**, *113*, 131.
 (77) States, D. J.; Haberkorn, R. A.; Ruben, D. J. *J. Magn. Reson.* **1982**, *48*, 286.
 (78) Earl, W. L.; VanderHart, D. L. *J. Magn. Reson.* **1982**, *48*, 35.
 (79) Morcombe, C. R.; Zilm, K. W. *J. Magn. Reson.* **2003**, *162*, 479.
 (80) Clark, S. J.; Segall, M. D.; Pickard, C. J.; Hasnip, P. J.; Probert, M. J.; Refson, K.; Payne, M. C. Z. *Kristallogr.* **2005**, *220*, 567.
 (81) Pickard, C. J.; Mauri, F. *Phys. Rev. B* **2001**, *63*, 245101.
 (82) Vanderbilt, D. *Phys. Rev. B* **1990**, *41*, 7892.
 (83) Yates, J. R.; Pickard, C. J.; Mauri, F. *Phys. Rev. B* **2007**, *76*, 024401.
 (84) Fletcher, D. A.; McMeeking, R. F.; Parkin, D. *J. Chem. Inf. Comput. Sci.* **1996**, *36*, 746.
 (85) Perdew, J. P.; Burke, K.; Ernzerhof, M. *Phys. Rev. Lett.* **1999**, *77*, 3865.

- (86) Sebastiani, D. *Chem. Phys. Chem.* **2006**, *7*, 164.
 (87) Gervais, C.; Dupree, R.; Pike, K. J.; Bonhomme, C.; Profeta, M.; Pickard, C. J.; Mauri, F. *J. Phys. Chem. A* **2005**, *109*, 6960.
 (88) Yates, J. R.; Pickard, C. J.; Payne, M. C.; Dupree, R.; Profeta, M.; Mauri, F. *J. Phys. Chem. A* **2004**, *108*, 6032.

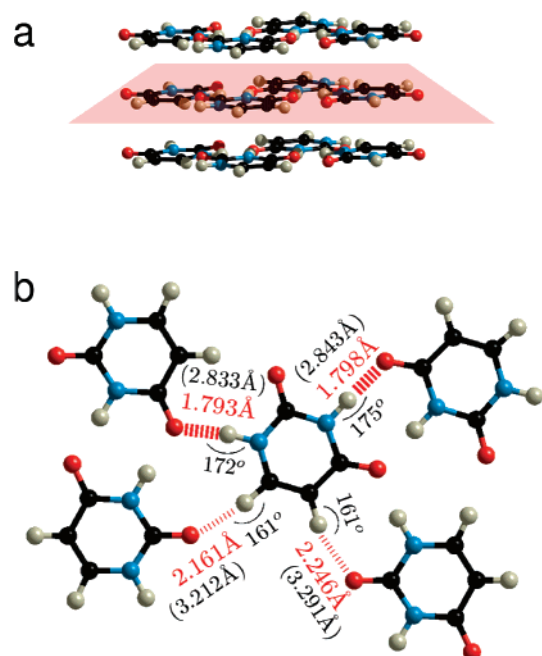


Figure 1. Crystal structure adopted by uracil. (a) Planar arrangement. (b) Conventional N–H···O and weak C–H···O hydrogen bonding within a plane. Color coding: C black, O red, N blue, H gray. The XHY angle, the H···X distance (in red), and the XY distance (in brackets) are indicated.

hydrogen were determined in uracil (similarly to procedures adopted in ref 51,53,87, and 88) and found to be $\sigma_{\text{ref}} = 29.7$ ppm for ^1H and $\sigma_{\text{ref}} = 167.8$ ppm for ^{13}C . The same reference shieldings were used for 4-cyano-4'-ethynylbiphenyl. More details on how the references are obtained are given in the Supporting Information. The shielding references for ^{17}O (water) and ^{15}N (nitromethane) were taken from ref 87, namely $\sigma_{\text{ref}} = -154.3$ for ^{15}N and $\sigma_{\text{ref}} = 261.5$ for ^{17}O . Note that these reference values were obtained using Trouiller–Martins norm-conserving pseudopotentials,⁸⁹ and hence care should be exercised when considering the ^{15}N and ^{17}O chemical shifts tabulated here. It is to be emphasized, however, that the changes in chemical shifts that are of primary interest in this study are independent of the reference value.

It should be noted that the NMR shielding contains, in principle, a contribution dependent on the sample shape arising from the effect of the bulk magnetic susceptibility. In common with previous GIPAW studies the shielding is computed for the case of a spherical sample. For such a geometry the observed shielding is independent of the bulk susceptibility. This is the most natural arrangement to quantify the intermolecular interactions; furthermore, it is directly applicable to magic-angle spinning experiments which eliminate the isotropic bulk magnetic susceptibility.⁹⁰

3. Results and Discussion

3.1. C–H···O Weak Hydrogen Bonding in Uracil. As shown in Figure 1, the X-ray single-crystal diffraction structure of uracil⁹¹ reveals a layered structure of planes stacked along (001) at a separation of 3.136 Å. There is one molecule in the asymmetric unit cell, with Figure 1b showing the intermolecular hydrogen bonding within each plane. Specifically, there are two distinct N–H···O hydrogen bonds to one carbonyl acceptor and two distinct C–H···O hydrogen bonds to the second carbonyl acceptor, with the H···O distances being 20–25% longer for the latter weak hydrogen bonds. The NHO bond angles are also

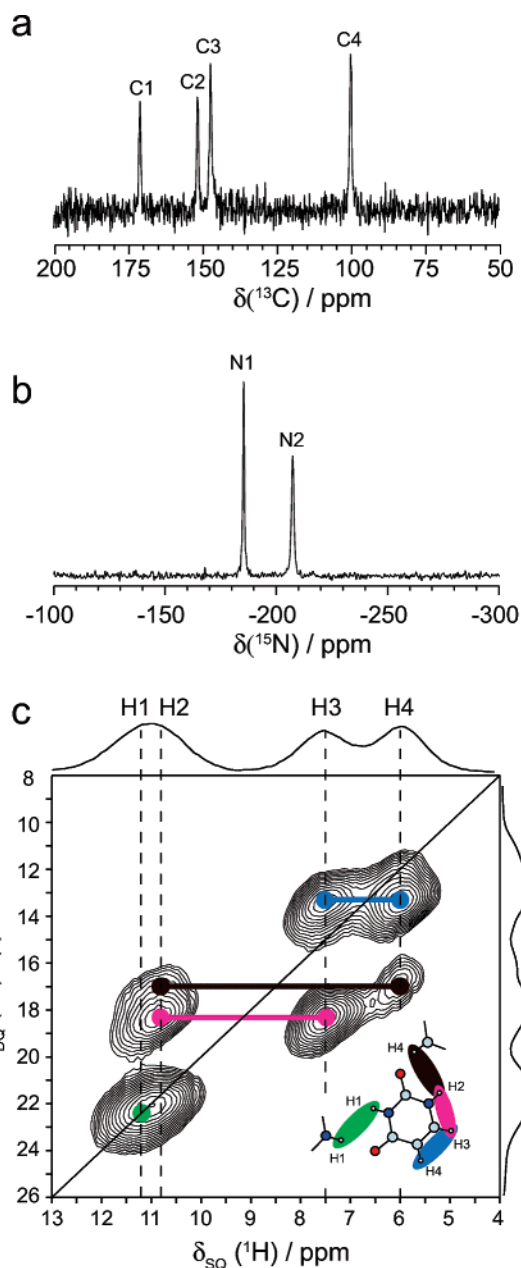


Figure 2. (a) ^{13}C (300 MHz) CP MAS (8.5 kHz), (b) ^{15}N (300 MHz) CP MAS (8.5 kHz), and (c) ^1H (600 MHz) DQ MAS (40 kHz) spectra of uracil (a,c) at natural abundance and (b) with ^{15}N labeling. The base contour is at 26% of the maximum intensity.

slightly closer to the ideal 180° than the CHO bond angles. Note that the bond lengths and angles given in Figure 1b are those obtained after geometry optimization, as described in the Computational Details (section 2.3).

Figure 2 presents a (a) ^{13}C CP MAS, (b) ^{15}N CP MAS, and (c) rotor-synchronized two-dimensional ^1H DQ MAS NMR spectrum of uracil (a,c) at natural abundance and (b) with ^{15}N labeling. Such a DQ spectrum displays DQ peaks for pairs of dipolar-coupled ^1H nuclei, where the DQ frequency is given by the sum of the single-quantum frequencies of the two involved protons, i.e., $\omega_{DQ} = \omega_{SQ1} + \omega_{SQ2}$. To a first approximation, the DQ peak intensity is proportional to the dipolar coupling squared; this corresponds to a $1/r^6$ distance dependence, and hence, for a typical organic solid, DQ peaks are only observed for pairs of protons with a close spatial

(89) Trouiller, N.; Martins, J. L. *Phys. Rev. B* **1991**, *43*, 1993.

(90) Harris, R. K.; Becker, E. D.; Cabral de Menezes, S.; Goodfellow, R.; Granger, P. *Pure Appl. Chem.* **2001**, *73*, 1795.

(91) Stewart, R. F.; Jensen, L. H. *Acta Crystallogr.* **1967**, *23*, 1102.

Table 1. Comparison of Experimental Solid-State NMR and Computed ^1H Chemical Shifts for Uracil

| donor and site | expt [ppm] | calcd ^a [ppm] | | | | $\Delta\delta_{\text{iso}}^{\text{plane-mol}}$ [ppm] | NICS [ppm] |
|-------------------|---------------|--------------------------|-------|-------------------|------------------------|---|---------------|
| | | cryst. | plane | mol. ^b | rel. mol. ^c | | |
| N–H H1 | 11.2 | 11.7 | 12.5 | 7.4 | 6.7 | 5.1 | 0.1 |
| N–H H2 | 10.8 | 11.2 | 11.9 | 6.5 | 5.8 | 5.4 | 0.01 |
| C–H H3 | 7.5 | 7.2 | 8.1 | 6.1 | 6.1 | 2.0 | 0.2 |
| C–H H4 | 6.0 | 5.5 | 6.3 | 4.1 | 4.0 | 2.2 | 0.3 |

^a $\delta_{\text{iso}} = \sigma_{\text{ref}} - \sigma_{\text{iso}}$, where $\sigma_{\text{ref}}(^1\text{H}) = 29.7$ ppm. ^b Geometry as that in optimized crystal structure. ^c Geometry after all atoms are relaxed.

proximity (less than 3.5 Å).^{26,28,92} In Figure 3c, pairs of cross-peaks are observed at 6.0 + 7.5 = 13.5 and 7.5 + 10.8 = 18.3 ppm corresponding to the intramolecular proximity of the H3 and H4 (2.53 Å, dipolar coupling constant $d_{jk} = 7.4$ kHz) and H2 and H3 (2.35 Å, $d_{jk} = 9.2$ kHz) protons, respectively. In addition, a diagonal peak at 11.2 + 11.2 = 22.4 ppm (2.44 Å, $d_{jk} = 8.3$ kHz) corresponding to the intermolecular proximity of two H1 protons is observed, while a pair of cross-peaks at 6.0 + 10.8 = 16.8 ppm (2.69 Å, $d_{jk} = 6.2$ kHz) corresponding to the intermolecular proximity of the H2 and H4 protons is also observed. The extension to two dimensions thus allows the assignment of the distinct H1 and H2 resonances that are not resolved in a one-dimensional spectrum.

Table 1 compares the experimental ^1H solid-state NMR chemical shifts with the results of first-principles calculations. Note that it is absolute shieldings that are determined in such first-principles calculations. To allow comparison with experimental chemical shifts, the calculated chemical shifts presented in Table 1 and elsewhere in this paper are determined with respect to a reference shielding, whose calculation is described in the Computational Details section. (The calculated absolute shieldings are given in the Supporting Information.) The experimental and calculated chemical shifts for the periodic crystal structure are in good agreement, with the largest discrepancies (± 0.5 ppm) seen for the lowest and highest values. This is a common observation for such calculations, which is linked to the fact that currently used density functionals are believed to overestimate the paramagnetic contribution to the chemical shift.⁹³

While solid-state NMR chemical shifts can only be determined experimentally for the case of powdered crystallites (or single crystals) corresponding to the periodic crystal structure, much greater flexibility is possible with calculations. For example, ref 51 compares ^1H chemical shifts of maltose anomers as calculated for, on the one hand, the full crystal structure and, on the other hand, isolated molecules extracted from the crystal structure; the isolated molecule to crystal changes in the ^1H chemical shift were shown to be a quantitative measure of the relative strength of $\text{CH}\cdots\text{O}$ weak hydrogen-bonding interactions. For uracil, insight into the effect of intermolecular interactions on the NMR chemical shifts is provided by a comparison of calculated ^1H chemical shifts (see Table 1) for the full periodic crystal with those calculated for an isolated plane or an isolated molecule (for the latter two cases, the isolated plane or molecule were extracted from the geometrically optimized crystal structure, and the chemical shifts were calculated without further

Table 2. Comparison of C–H and N–H Bond Lengths Obtained from a Geometry Optimization of Uracil within Its Periodic Crystal Structure and as an Isolated Molecule

| bond | bond lengths (in Å) | |
|-------|---------------------|------------------------|
| | cryst. | rel. mol. ^a |
| N1–H1 | 1.047 | 1.024 |
| N2–H2 | 1.046 | 1.020 |
| C3–H3 | 1.090 | 1.088 |
| C4–H4 | 1.087 | 1.086 |

^a All atoms relaxed.

geometric optimization). The ^1H chemical shift differences between the crystal and an isolated plane are less than 1 ppm, as is to be expected for the weak aromatic character of uracil.⁹⁴ These small changes are to be compared with previously reported calculated ^1H chemical shift differences due to intermolecular ring currents of up to 6 ppm for benzene, naphthalene, hexabenzocoronene, and imidazole aromatic moieties.^{41–43,56,57,59,64}

In order to separate out the effect of interplane aromatic ring currents, a comparison is made here between calculations for an isolated molecule and an isolated plane of molecules. The molecule to plane differences defined by $\Delta\delta_{\text{iso}}^{\text{plane-mol}} = \delta_{\text{iso}}^{\text{plane}} - \delta_{\text{iso}}^{\text{mol}}$ are listed for the NH and CH ^1H nuclei in Table 1. Of particular interest is a comparison of the $\Delta\delta_{\text{iso}}^{\text{plane-mol}}$ values for the NH protons, H1 and H2, involved in conventional $\text{NH}\cdots\text{O}$ hydrogen bonding interactions, with those for the CH protons, H3 and H4, involved in weak $\text{CH}\cdots\text{O}$ hydrogen bonding interactions. It is well-known that the ^1H chemical shift is a sensitive indicator of hydrogen-bonding strength,^{95–97} and hence the $\Delta\delta_{\text{iso}}^{\text{plane-mol}}$ values of over 5 ppm for the NH protons are unsurprising. A similar change has been noted by Schmidt et al. for a NH proton of L-histidine·HCl·H₂O involved in $\text{NH}\cdots\text{O}$ intermolecular hydrogen bonding.⁵⁶ For the CH protons involved in weak $\text{CH}\cdots\text{O}$ hydrogen bonding interactions, $\Delta\delta_{\text{iso}}^{\text{plane-mol}}$ values of over 2 ppm are calculated, i.e., the changes are $\sim 40\%$ of those for the conventional $\text{NH}\cdots\text{O}$ hydrogen bonding interactions. This will be surprising to many NMR spectroscopists, since there is very little discussion of the effect of weak hydrogen bonding on NMR chemical shifts in the literature.^{10,24,51,98} These $\Delta\delta_{\text{iso}}^{\text{plane-mol}}$ values of 2.0–2.2 ppm are slightly larger than the biggest molecule to crystal changes in the ^1H chemical shift as calculated for the CH protons in maltose anomers (1.9 ppm)⁵¹ that also exhibit $\text{CH}\cdots\text{O}$ weak hydrogen bonding.

The $\Delta\delta_{\text{iso}}^{\text{plane-mol}}$ values in Table 1 are calculated by comparison to the case of an isolated molecule extracted from the geometrically optimized crystal structure without further geometric optimization. In this way, the above method does not consider the effect of intermolecular hydrogen-bonding interactions on the YH bond lengths. In order to address this, Table 2 compares the YH bond lengths for uracil molecules for the case of geometric optimizations of the periodic crystal structure or an isolated molecule (see computational details). It is observed that while the N–H bonds are ~ 0.02 Å longer for the periodic

(94) Vernon, G. S. B.; Fleumingue, J.-M. *J. Mol. Model.* **2001**, *7*, 334.

(95) Berglund, B.; Vaughan, R. W. *J. Chem. Phys.* **1980**, *73*, 2037.

(96) Jeffrey, G. A.; Yeon, Y. *Acta Crystallogr.* **1986**, *B42*, 410.

(97) Harris, R. K.; Jackson, P.; Merwin, L. H.; Say, B. J.; Hagele, G. *J. Chem. Soc., Faraday Trans.* **1988**, *84*, 3649.

(98) Scheffer, J. R.; Wong, Y.-F.; Patil, A. O.; Curtin, D. Y.; Paul, I. C. *J. Am. Chem. Soc.* **1985**, *107*, 4898.

(92) Schnell, I.; Spiess, H. W. *J. Magn. Reson.* **2001**, *151*, 153.

(93) Buhl, M.; Kaupp, M.; Malkina, O. L.; Malkin, V. G. *J. Comput. Chem.* **1999**, *20*, 91.

crystal as opposed to the relaxed isolated molecule, the C–H bonds change by no more than 0.002 Å. Note that similar observations have been made from geometrical data calculated in quantum-chemical studies that compare uracil in the gas phase with either a uracil–uracil dimer (UU7)⁹⁹ or a cluster representing the uracil periodic crystal.¹⁰⁰ The ¹H chemical shifts determined for the geometrically relaxed isolated molecule are also listed in Table 1. It is evident that while the ~0.02 Å change in the NH bond length leads to a 0.7 ppm change for the NH protons as compared to the calculation for an isolated molecule extracted from the crystal structure without further optimization, there is virtually no change (<0.1 ppm) for the CH protons associated with only a 0.002 Å change in the CH bond length.

While the calculation of $\Delta\delta_{\text{iso}}^{\text{plane-mol}}$ excludes ring current effects caused by the other planes above and below, there remains potential contributions to $\Delta\delta_{\text{iso}}^{\text{plane-mol}}$ arising from ring currents in neighboring, in-plane molecules. One approach that has been previously employed to untangle hydrogen bonding and aromatic ring current effects is the modeling of the latter as a single-point dipole. White et al.¹⁰¹ used this approach together with a set of susceptibility data to interpret experimentally observed ¹H chemical shifts of zeolite OH protons involved in hydrogen bonding to pi-rich adsorbates such as acetylene and ethylene. In the context of the present work a first-principles approach is however to be preferred, and the ring current contributions can be easily evaluated by calculating the in-plane Nucleus Independent Chemical Shifts (NICSS). By definition, the NICSS is minus the isotropic shielding, which in principle can be calculated at any site, whether the site is occupied by a nucleus or not. NICSS calculations are finding increasing application in the interpretation of solid-state NMR parameters.^{56,63,86,102–104} For the uracil NICSS calculations, one molecule was removed from the unit cell for the plane, and the NICSSs due to the other three molecules were calculated at the positions of the removed molecule. The corresponding NICSSs at the hydrogen sites are given in the last column of Table 1. While the in-plane NICSSs values are small (at most 0.3 ppm), their sign indicates that $\Delta\delta_{\text{iso}}^{\text{plane-mol}}$ tends to overestimate slightly the strength of the intermolecular hydrogen bonding interactions in uracil.

Table 3 presents the results of analogous chemical shift calculations for the ¹³C, ¹⁵N, and ¹⁷O nuclei. Note that the stated calculated chemical shifts were again determined with respect to a reference shielding (see Computational Details). While the $\Delta\delta_{\text{iso}}^{\text{plane-mol}}$ values for the ¹H nuclei are positive (see Table 1), the $\Delta\delta_{\text{iso}}^{\text{plane-mol}}$ values are negative for the hydrogen-bond acceptor ¹⁷O nuclei (Table 3), i.e., corresponding to a substantial increase in shielding when comparing the shieldings for an isolated molecule to that for a plane. Moreover, the molecule to plane change for the acceptor of two conventional NH···O hydrogen bonds, O1, is about 4.5 times bigger than that for O2, which participates in two CH···O weak hydrogen bonds. This marked difference in ¹⁷O chemical shifts has been noted

Table 3. Comparison of Experimental Solid-State NMR and Computed ¹³C, ¹⁵N, and ¹⁷O Chemical Shifts for Uracil

| site | expt [ppm] | calcd ^b shift [ppm] | | | | $\Delta\delta_{\text{iso}}^{\text{plane-mol}}$ [ppm] | NICS [ppm] |
|---------|------------------|--------------------------------|--------|-------------------|------------------------|--|------------|
| | | cryst. | plane | mol. ^c | rel. mol. ^d | | |
| C1 C=O | 170.9 | 169.6 | 170.3 | 165.0 | 159.9 | 5.3 | 0.6 |
| C2 C=O | 151.7 | 149.8 | 150.7 | 148.2 | 147.0 | 2.5 | 0.4 |
| C3 C–H | 147.0 | 149.1 | 148.3 | 138.4 | 137.6 | 9.9 | 0.3 |
| C4 C–H | 99.9 | 100.0 | 99.2 | 100.7 | 101.7 | –1.5 | 0.3 |
| N1 | –185.2 | –209.2 | –209.6 | –208.9 | –211.6 | –0.7 | 0.5 |
| N2 | –207.3 | –225.2 | –226.8 | –244.2 | –245.7 | 17.4 | 0.3 |
| O1 (NH) | 275 ^a | 274.4 | 273.2 | 407.8 | 379.0 | –134.6 | 1.0 |
| O2 (CH) | 245 ^a | 257.6 | 256.0 | 286.0 | 274.8 | –30.0 | 0.6 |

^a Reference 100. ^b $\delta_{\text{iso}} = \sigma_{\text{ref}} - \sigma_{\text{iso}}$, where $\sigma_{\text{ref}}(^{13}\text{C}) = 167.8$ ppm, $\sigma_{\text{ref}}(^{15}\text{N}) = -154.3$ ppm (ref 87), and $\sigma_{\text{ref}}(^{17}\text{O}) = 261.5$ ppm (ref 87). ^c Geometry as that in optimized crystal structure. ^d Geometry after all atoms are relaxed.

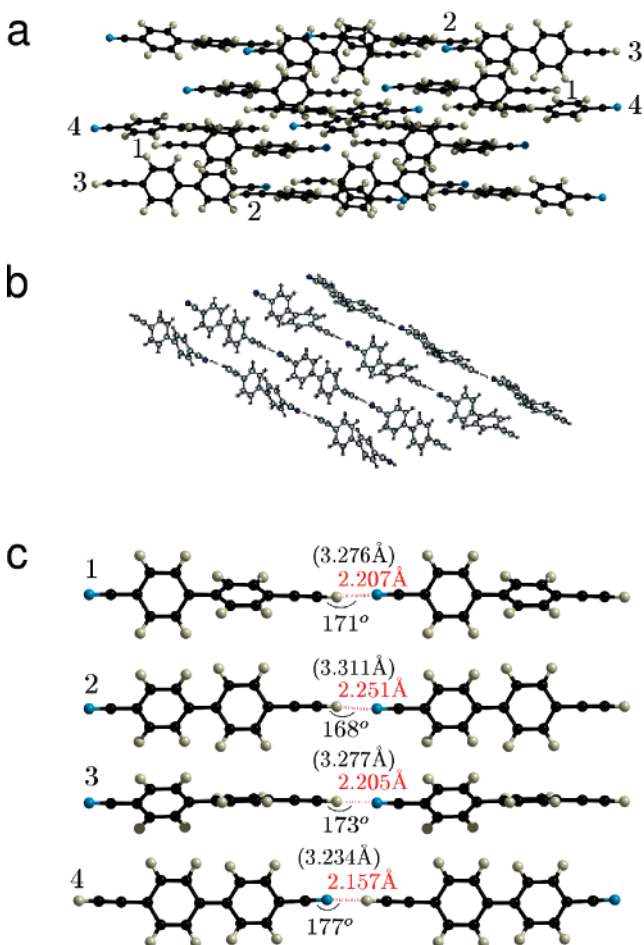


Figure 3. Packing of 4-cyano-4'-ethynylbiphenyl molecules in the solid state, as determined by X-ray single-crystal diffraction.⁶⁵ (a) The four molecules of the asymmetric unit cell are labeled. (b) View of the four distinct chains. (c) Postulated C–H···N weak hydrogen bonding. Color coding: C black, N blue, H gray. The CHN angle, the HN distance (in red), and the CN distance as obtained after geometry optimization (see Computational Details (section 2.3)) are indicated.

(99) Pavel, H.; Šponer, J.; Cubero, E.; Orzoco, M.; Luque, F. J. *J. Phys. Chem. B* **2000**, *104*, 6286.

(100) Ida, R.; De Clerck, M.; Wu, G. *J. Phys. Chem. A* **2006**, *110*, 1065.

(101) White, J. L.; Beck, L. W.; Haw, J. F. *J. Am. Chem. Soc.* **1992**, *114*, 6182.

(102) Rapp, A.; Schnell, I.; Sebastiani, D.; Brown, S. P.; Percec, V.; Spiess, H. W. *J. Am. Chem. Soc.* **2003**, *125*, 13284.

(103) Facelli, J. C. *Magn. Reson. Chem.* **2006**, *44*, 401.

(104) Ma, Z.; Halling, M. D.; Solum, M. S.; Harper, J. K.; Orendt, A. M.; Facelli, J. C.; Pugmire, R. J.; Grant, D. M.; Mick, A. W.; Scott, L. T. *J. Phys. Chem. A* **2007**, *111*, 2020.

previously by Ida et al. who compared quantum-chemical calculations for clusters of uracil molecules with that for an isolated uracil molecule.¹⁰⁰ The sensitivity of the ¹⁷O chemical shift and also quadrupolar interaction to hydrogen bonding has been noted by Wu and co-workers also for secondary amides, benzamide, urea,^{105–107} and guanine and guanosine derivatives.¹⁰⁸ For the ring carbon and nitrogen atoms, there are no

clear trends in the molecule to plane changes in chemical shifts; this is presumably a consequence of the delocalization of the electrons in the uracil ring.

3.2. C–H···N Weak Hydrogen Bonding in 4-Cyano-4'-ethynylbiphenyl. The above section considered weak hydrogen bonding between an sp^2 hybridized aromatic CH donor and a C=O carbonyl acceptor; this section considers **2**, where the X-ray single-crystal structure⁶⁵ suggests weak hydrogen bonding between an sp hybridized C≡CH donor and a C≡N acceptor. As shown in Figure 3a, the packing is centro-symmetric, with four molecules in the asymmetric unit cell, labeled 1–4 in Figure 3a. The crystal structure shows that the molecules pack as four repeating chains (see Figure 3) corresponding to the four molecules of the asymmetric unit cell; the chains are all aligned along (010), noting that chain 4 is oriented in the opposite direction. Reference 65 indicates significant orientational disorder for chain 2, with a stated probability of 40% for the chain to be oriented in the opposite direction to that in the structure deposited in the Cambridge Crystal Database.⁸⁴ The H···N and CN distances, as well as the CHN angles for the postulated intermolecular C–H···N weak hydrogen bonds corresponding to the four chains are indicated in Figure 3c. The stated distances and angles are those determined after full geometry optimization (see section 2.3).

Experimental ^1H , ^{13}C , and ^{15}N MAS NMR spectra of **2** are presented in Figures 4 and 5. Specifically Figure 4 presents (a,b) ^{13}C and (d) ^{15}N CP MAS spectra of **2** at (a) natural abundance and (b, d) with $^{13}\text{C}\equiv^{13}\text{CH}$ and $\text{C}\equiv^{15}\text{N}$ labeling, while Figure 5 presents (a) a one-dimensional MAS and (b) a two-dimensional DQ MAS ^1H spectrum of **2**. The horizontal bar in Figure 5b indicates DQ coherences between an ethynyl proton (H9) and an aromatic proton; the selected slices extracted at different DQ frequencies shown in Figure 5c indicate a range of positions of the peak maxima corresponding to the ethynyl proton (H9), as is to be expected for the presence of four distinct molecules in the crystal structure.

The ^1H , ^{13}C , and ^{15}N chemical shifts were calculated for the periodic crystal structure (after geometric optimization) of **2**. Specifically, Tables 4 and 5 list the calculated ^1H , ^{13}C , and ^{15}N chemical shifts (again presented as relative shieldings with respect to the same calculated reference shieldings as used for uracil; see Computational Details) for the CH donor and N acceptor atoms of the $\text{C}\equiv\text{CH}\cdots\text{N}\equiv\text{C}$ hydrogen bonding arrangements (a full listing of the calculated absolute shieldings is given in the Supporting Information). Simulated spectra corresponding to the calculated ^{13}C and ^1H chemical shifts for the 15 carbon and 9 hydrogen atoms in each of the four distinct molecules are shown in Figures 4c and 5a (dashed line), respectively. Reasonable agreement between experiment and calculation is observed. For the ethynyl proton, H9, the calculated chemical shifts of 4.6, 4.0, 4.9, 4.8 ppm for molecule 1 to 4, respectively, are overestimated as compared to the experimental distribution of 3.3 to 3.8 ppm (see Figure 5b,c). Several factors potentially contribute to this overestimation: One may be the problem of DFT overestimating the paramagnetic contribution⁹³ noted above in the discussion of Table 1 for uracil;

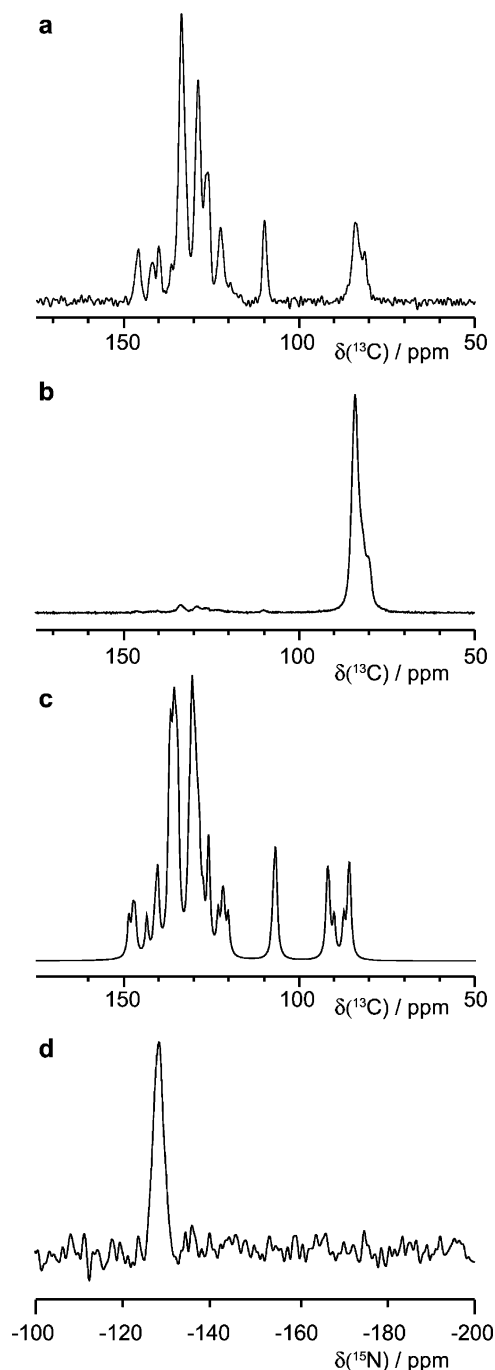


Figure 4. Experimental (a,b) ^{13}C and (d) ^{15}N CP MAS (8.5 kHz) NMR (300 MHz) spectra of 4-cyano-4'-ethynylbiphenyl (a) at natural abundance and (b, d) with $^{13}\text{C}\equiv^{13}\text{CH}$ and $\text{C}\equiv^{15}\text{N}$ labeling. The simulated spectrum (c) corresponds to the calculated chemical shifts for the 15 carbon nuclei in each of the four distinct molecules (tabulated in the Supporting Information) using Lorentzian lines with full width at half-maximum height of 0.5 ppm.

Another is the stated disorder in the crystal structure, upon which (after geometrical optimization) the chemical shift calculations are based.

In the following, an analogous approach to that employed for the case of uracil is adopted in order to quantify the effect of $\text{C}\equiv\text{CH}\cdots\text{N}\equiv\text{C}$ weak hydrogen bonding on the NMR chemical shifts for 4-cyano-4'-ethynylbiphenyl, focusing first on the ethynyl H9 ^1H chemical shifts. As noted above, the crystal structure reveals the formation of four distinct chains due to

(105) Yamada, K.; Dong, S.; Wu, G. *J. Am. Chem. Soc.* **2000**, *122*, 11602.

(106) Wu, G.; Yamada, K.; Dong, S.; Grondey, H. *J. Am. Chem. Soc.* **2000**, *122*, 4215.

(107) Dong, S.; Ida, R.; Wu, G. *J. Phys. Chem. A* **2000**, *104*, 11194.

(108) Kwan, I. C. M.; Mo, X.; Wu, G. *J. Am. Chem. Soc.* **2007**, *129*, 2398.

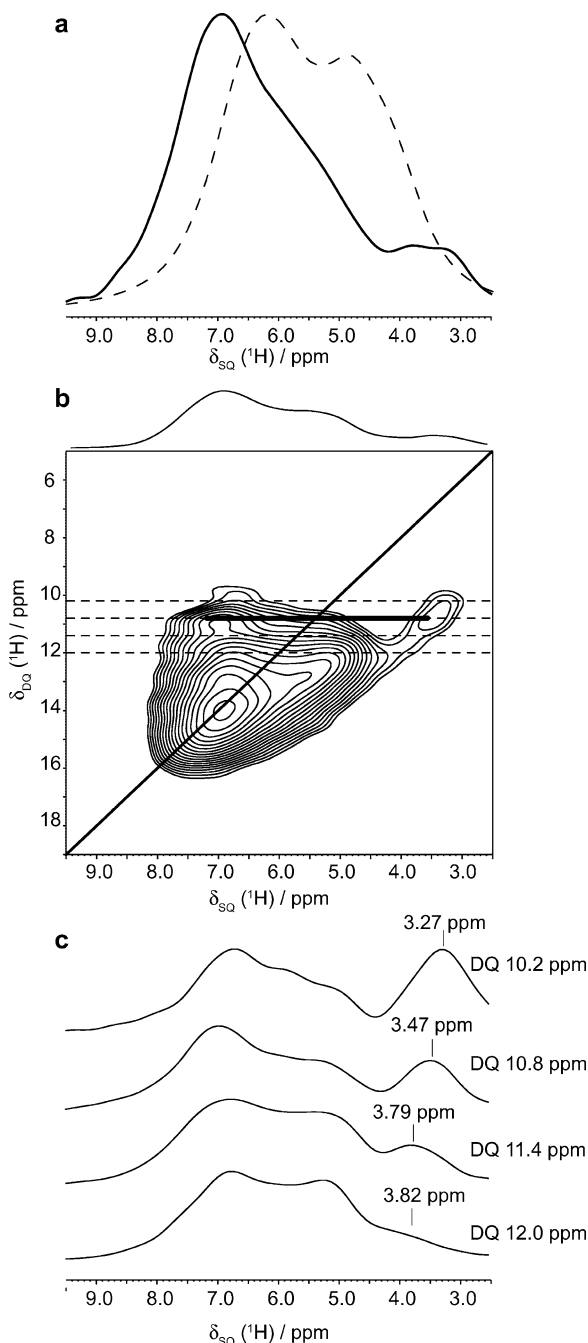


Figure 5. (a, solid line) A one-dimensional MAS and (b) a two-dimensional DQ MAS ^1H (600 MHz) NMR spectrum of 4-cyano-4'-ethynylbiphenyl, recorded at a MAS frequency of 40 kHz. In (a), the dashed line is a simulated spectrum that corresponds to the calculated chemical shifts for the nine hydrogen nuclei in each of the four distinct molecules (tabulated in the Supporting Information), using Lorentzian lines with full width at half-maximum height of 0.5 ppm. The horizontal bar in (b) indicates DQ coherences between an ethynyl proton (H9) and an aromatic proton; selected slices extracted at different DQ frequencies are indicated in (c), with the positions of the peak maxima corresponding to the ethynyl proton (H9) being specified.

the linking together of the individual molecules via intermolecular weak hydrogen bonding. It is, therefore, informative to consider chemical shifts calculated for the four isolated chains (as extracted from the geometrically optimized crystal structure, with the chemical shifts being calculated without further geometric optimization). Table 4 reveals only small differences in the calculated crystal and chain H9 ^1H chemical shifts; this

Table 4. Computed ^1H Chemical Shifts of H9 (C \equiv CH) in 4-Cyano-4'-ethynylbiphenyl

| mol label | calcd ^a shift [ppm] | | | | $\Delta\delta_{\text{iso}}^{\text{chain-mol}}$ [ppm] | NICS [ppm] |
|-----------|--------------------------------|-------|-------------------|------------------------|--|------------|
| | cryst. | chain | mol. ^b | rel. mol. ^c | | |
| 1 | 4.6 | 4.5 | 3.3 | 3.1 | 1.2 | -0.9 |
| 2 | 4.0 | 4.4 | 3.3 | 3.2 | 1.1 | -0.8 |
| 3 | 4.9 | 4.6 | 3.4 | 3.2 | 1.2 | -0.9 |
| 4 | 4.8 | 4.8 | 3.4 | 3.2 | 1.4 | -1.0 |

^a $\delta_{\text{iso}} = \sigma_{\text{ref}} - \sigma_{\text{iso}}$, where $\sigma_{\text{ref}}(^1\text{H}) = 29.7$ ppm (uracil reference). ^b Geometry as that in optimized crystal structure. ^c Geometry after protons are relaxed.

Table 5. Computed C and N Chemical Shifts of C15 (C \equiv ^{13}C H) and $^{15}\text{N}1$ ($^{13}\text{C}\equiv^{15}\text{N}$) in 4-Cyano-4'-ethynylbiphenyl

| mol and site label | calcd ^a shift [ppm] | | | | $\Delta\delta_{\text{iso}}^{\text{chain-mol}}$ [ppm] | NICS [ppm] |
|--------------------|--------------------------------|-------|-------------------|------------------------|--|------------|
| | cryst. | chain | mol. ^b | rel. mol. ^c | | |
| 1 C15 | 92.0 | 90.4 | 80.3 | 80.0 | 10.2 | -0.3 |
| 2 C15 | 90.2 | 90.5 | 80.8 | 80.5 | 9.8 | -0.3 |
| 3 C15 | 91.6 | 91.1 | 80.7 | 80.4 | 10.4 | -0.3 |
| 4 C15 | 92.2 | 93.0 | 81.5 | 81.3 | 11.5 | -0.3 |
| 1 N1 | -103.0 | -95.0 | -82.8 | -82.9 | -12.2 | 0.2 |
| 2 N1 | -101.7 | -94.9 | -83.2 | -83.3 | -11.6 | 0.2 |
| 3 N1 | -101.1 | -95.6 | -83.1 | -83.2 | -12.4 | 0.2 |
| 4 N1 | -99.8 | -96.6 | -83.2 | -82.2 | -13.5 | 0.2 |

^a $\delta_{\text{iso}} = \sigma_{\text{ref}} - \sigma_{\text{iso}}$, where $\sigma_{\text{ref}}(^{13}\text{C}) = 167.8$ ppm (uracil reference) and $\sigma_{\text{ref}}(^{15}\text{N}) = -154.3$ ppm (ref 87). ^b Geometry as that in optimized crystal structure. ^c Geometry after protons are relaxed.

is consistent with a packing that exposes the C \equiv CH moieties to minimal interchain ring current effects. As shown in the Supporting Information, larger chain to crystal changes in the ^1H chemical shift (up to 2.6 ppm) are observed for hydrogen atoms on the benzene rings.

Table 4 also lists the H9 ^1H chemical shifts calculated for the case of extracting the four distinct isolated molecules from the geometrically optimized crystal structure. Calculations were performed without and with further geometric optimization of the isolated molecule structures. Such further geometric optimization resulted in changes in the CH bond length from 1.078, 1.076, 1.078, 1.078 Å (without optimization) to 1.069, 1.069, 1.070, 1.069 Å (optimized); as shown in Table 4, such small changes of <1% in the CH bond length led to changes of at most only 0.2 ppm in the H9 ^1H chemical shifts. For the H9 proton, the molecule to chain changes, $\Delta\delta_{\text{iso}}^{\text{chain-mol}} = \delta_{\text{iso}}^{\text{mol}} - \delta_{\text{iso}}^{\text{chain-mol}}$, are between 1.1 and 1.4 ppm. For the other hydrogen atoms on the benzene rings, $|\Delta\delta_{\text{iso}}^{\text{chain-mol}}|$ is at most 0.1 ppm (see Supporting Information).

While interchain ring current effects are excluded by calculating the chemical shifts for the isolated chain, it is necessary to consider any ring current effects due to adjacent molecules within each chain. To this end, every other molecule was removed from each chain and the intrachain NICSs were calculated at the relevant position in the removed molecule. As shown in Table 4, the intrachain NICSs for H9 range from 0.8 to 1 ppm. These intrachain NICSs are larger in magnitude and of different sign, i.e., positive as opposed to negative, as compared to the in-plane NICSs calculated for uracil (see Table 1). For 4-cyano-4'-ethynylbiphenyl, the calculated intrachain NICSs for H9, thus, indicate that $\Delta\delta_{\text{iso}}^{\text{chain-mol}}$ underestimates the chemical shift change due to intermolecular weak hydrogen bonding by about 1 ppm.

Table 6. A Comparison of CH...X Weak Hydrogen Bonding in Maltose, Uracil, and 4-Cyano-4'-ethynylbiphenyl

| donor | acceptor | dist. [Å] H...X | dist. [Å] CX | ∠ (deg) CHX | $\Delta\delta_{\text{iso}}(^1\text{H})$ (estim. corr. ^a) [ppm] |
|------------------------------------|----------|--------------------|-----------------|----------------|--|
| ^a C(sp ³)-H | OH | 2.479 | 3.564 | 167 | 1.9 |
| ^a C(sp ³)-H | OH | 2.479 | 3.564 | 168 | 1.9 |
| ^b C(sp ²)-H | C=O | 2.161 | 3.212 | 161 | 2.0 (-0.2) |
| ^b C(sp ²)-H | C=O | 2.246 | 3.291 | 161 | 2.2 (-0.3) |
| ^c C(sp)-H | C≡N | 2.157 | 3.234 | 177 | 1.4 (+1.0) |
| ^c C(sp)-H | C≡N | 2.205 | 3.277 | 173 | 1.2 (+0.9) |
| ^c C(sp)-H | C≡N | 2.207 | 3.276 | 171 | 1.2 (+0.9) |
| ^c C(sp)-H | C≡N | 2.251 | 3.311 | 168 | 1.1 (+0.8) |

^a Maltose, $\Delta\delta_{\text{iso}} = \delta_{\text{iso}}^{\text{cryst}} - \delta_{\text{iso}}^{\text{mol}}$, from ref 51. ^b Uracil, $\Delta\delta_{\text{iso}} = \delta_{\text{iso}}^{\text{plane}} - \delta_{\text{iso}}^{\text{mol}}$. ^c 4-Cyano-4'-ethynylbiphenyl, $\Delta\delta_{\text{iso}} = \delta_{\text{iso}}^{\text{chain}} - \delta_{\text{iso}}^{\text{mol}}$. ^d -NICS.

In 4-cyano-4'-ethynylbiphenyl, each C≡CH donor and each C≡N acceptor are only involved in one weak hydrogen bond; this coupled with the fact that the donor and acceptor groups are well separated within each molecule means that the chain to molecule changes $\Delta\delta_{\text{iso}}^{\text{chain-mol}}$ for the heteroatoms are also expected to be clearly interpretable measures of the strength of the weak hydrogen-bonding interactions. The calculated ¹³C and ¹⁵N chemical shifts for the CH donor and N acceptor atoms of the C≡CH...N≡C hydrogen bonding arrangements are listed in Table 5. $\Delta\delta_{\text{iso}}^{\text{chain-mol}}$ for the CH carbon C15 (attached to H9) varies from 9.8 to 11.5 ppm; this compares to $\Delta\delta_{\text{iso}}^{\text{chain-mol}}$ for the other carbon nuclei of less than 3.4 ppm (see Supporting Information). For the ¹⁵N nuclei of the hydrogen-bond acceptor C3N, $\Delta\delta_{\text{iso}}^{\text{chain-mol}}$ are of similar magnitude but of opposite sign, varying from -11.6 to -13.5 ppm. Negative $\Delta\delta_{\text{iso}}^{\text{chain-mol}}$ values were also observed for the ¹⁷O nuclei of the hydrogen-bond acceptor carbonyl groups in uracil (see Table 3). Note that the intrachain NICSs (magnitudes of less than 0.3 ppm) in Table 5 are observed to be small as compared to the $\Delta\delta_{\text{iso}}^{\text{chain-mol}}$ values.

4. Conclusions

Weak CH...X hydrogen bonding in uracil and 4-cyano-4'-ethynylbiphenyl involves sp² and sp hybridized CH donor groups, respectively. Table 6 compares the relevant changes in the calculated ¹H chemical shift that are indicative of weak hydrogen-bonding strength for uracil ($\Delta\delta_{\text{iso}}^{\text{plane-mol}}$) and 4-cyano-4'-ethynylbiphenyl ($\Delta\delta_{\text{iso}}^{\text{chain-mol}}$). The table also lists the

results for the two strongest weak hydrogen bonds found in the maltose anomers ($\Delta\delta_{\text{iso}}^{\text{cryst-mol}}$) studied in ref 51. For uracil and 4-cyano-4'-ethynylbiphenyl, it is necessary to take into account the contribution of intermolecular ring currents to the ¹H chemical shift: the estimated corrections listed in the final column of Table 6 correspond to the negative of the intraplane and intrachain NICS values (see Tables 1 and 4). Note that there are no aromatic moieties in maltose and such a correction is, thus, not required. When these ring-current corrections are included, it is observed that the largest corrected $\Delta\delta_{\text{iso}}(^1\text{H})$ values are found for the weak hydrogen bonds in the sp hybridized case of 4-cyano-4'-ethynylbiphenyl. While this agrees with the predicted dependence on hybridization, i.e., C(sp)-H ≥ C(sp²)-H ≥ C(sp³)-H, 1,13,17 the $\Delta\delta_{\text{iso}}(^1\text{H})$ values are in fact very similar (~2 ppm) for all the considered weak CH...X hydrogen bonds, suggesting only a weak dependence on hybridization (at least for the small set of compounds considered in this study).

All the weak CH...X hydrogen bonds considered here correspond to short H...X distances (<2.5 Å) and CHX angles close to linearity (>160°). For such favorable weak hydrogen-bonding geometries, the bonding interactions make a significant contribution (~2 ppm for ¹H, >10 ppm for ¹³C, ¹⁵N, and ¹⁷O) to the observed chemical shift that must be taken account of when interpreting NMR spectra. Where geometries are less favorable, the chemical shift changes due to weak hydrogen-bonding could still be significant, but a careful case-by-case investigation is to be recommended.

Acknowledgment. Funding from EPSRC (U.K.) is acknowledged, including the use of the EPSRC Chemical Database Service. Computational work was carried out at the Centre for Scientific Computing at the University of Warwick (SRIF funded) and the EaStCHEM Research Computing Facility at the University of St Andrews. Support from the Estonian Science Foundation and EU FP6 UPMAN project is acknowledged.

Supporting Information Available: Tables of all calculated absolute shieldings (PDF) and geometrically optimized crystal structures (plain text). This material is available free of charge via the Internet at <http://pubs.acs.org>.

JA075892I